ACS APPLIED MATERIALS & INTERFACES

Research Article

www.acsami.org

Design of Polymer-Brush-Grafted Magnetic Nanoparticles for Highly Efficient Water Remediation

Aleeza Farrukh,[†] Attia Akram,[§] Abdul Ghaffar,[§] Sara Hanif,[‡] Almas Hamid,[‡] Hatice Duran,[ξ] and Basit Yameen*,[†]

[†]Department of Chemistry, School of Science and Engineering, Lahore University of Management Sciences, Lahore-54792, Pakistan

[ξ]Department of Materials Science & Nanotechnology Engineering, TOBB University of Economics and Technology, Sogutozu Cad. 43, 06560 Ankara, Turkey

[§]Department of Chemistry, University of Engineering and Technology, Lahore, Pakistan

[‡]Department of Environmental Sciences, Kinnaird College for Women, 93-Jail Road, Lahore, Pakistan

Supporting Information

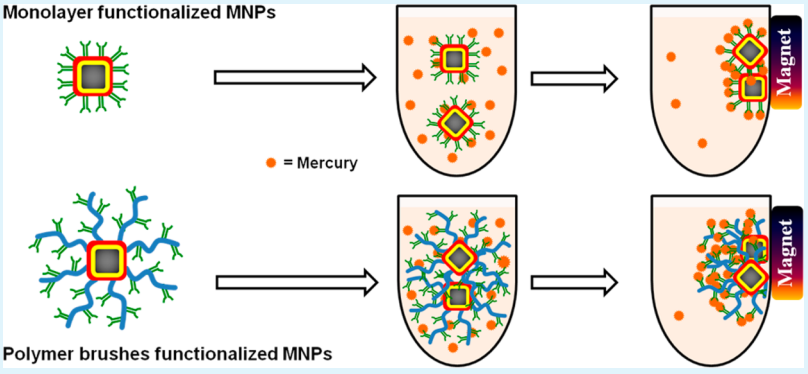

ABSTRACT: Highly efficient removal of mercury(II) ions (Hg^{II}) from water has been reported by employing polymer-brush-functionalized magnetic nanoparticles (MNPs). Surface-initiated conventional radical polymerization (SI-cRP) was used to grow poly(2-aminoethyl methacrylate hydrochloride) (poly-AEMA·HCl) polymer chains on magnetite nanoparticles (Fe_3O_4), followed by the transformation of pendant amino groups into dithiocarbamate (DTC) groups, which showed high chelating affinity toward Hg^{II} ions. This polymer-brush-based DTC-functionalized MNP (MNPs-polyAEMA·DTC) platform showed the complete removal of Hg^{II} from aqueous solutions. The Hg^{II} ion removal capacity and efficiency of MNPs-polyAEMA·DTC were compared with its monolayer analogue, which was derived from the direct transformation of amino groups of (3-aminopropyl) triethoxysilane (APTES)-functionalized MNPs (MNPs-APTES) to DTC functional groups (MNPs-DTC). The surface chemical modifications and higher chelating functional group density, in the case of MNPs-polyAEMA·DTC, were ascertained by transmission electron microscopy (TEM), thermogravimetric analysis (TGA), physical property measurement system (PPMS), attenuated total reflectance infrared (ATR-IR) spectroscopy, and X-ray photoelectron spectroscopy (XPS). The Hg^{II} ion removal capacity and efficiency of monolayer and polymer-brush-based DTC-functionalized MNPs (MNPs-DTC and MNPs-polyAEMA·DTC, respectively) were evaluated and compared by studying the effect of various factors on the percentage removal of Hg^{II} such as adsorbent amount, temperature, and contact time. Furthermore, the adsorption behavior of MNPs-DTC and MNPs-polyAEMA·DTC was analyzed by applying Langmuir and Freundlich adsorption isotherm models. In addition, the adsorption thermodynamics, as well as the adsorption kinetics, were also evaluated in detail. The higher surface functional group density of MNPs-polyAEMA·DTC led to superior remediation characteristics toward Hg^{II} ions than its monolayer analogue.

KEYWORDS: *magnetic nanoparticles, polymer brushes, dithiocarbamate, mercury, adsorbent*

INTRODUCTION

Over the years, the contamination of water with toxic heavy-metal ions has remained a matter of great concern. Emissions of hazardous substances to the aquatic environment can occur at every stage of their life cycle, from production, processing, and use by the general public, to their eventual disposal. In context of the toxic metals, mercury is considered to be the most toxic one, after plutonium.[1] The soluble bivalent form of mercury (Hg^{II}) pollutes a huge amount of fresh water, seawater, and under-groundwater bodies and soil. Bioaccumulation and biomagnification of mercury results in severe mercury poisoning, which affects the liver, kidney, brain, and lungs in humans.[2]

Received: January 31, 2013
Accepted: April 9, 2013
Published: April 9, 2013

Another particular concern is the potential developmental defects in children exposed to mercury in utero.[3] Therefore, even in minute traces, mercury pollution poses serious threats to the aquatic organisms and human beings.[4] As a result, mercury and its derivatives are classified as priority hazardous substances (PHSs) by several international environmental organizations, such as European Union Environmental Quality Standards Directives (EQSD)[5] and the United Nations Environment Programme (UNEP).[6] Consequently, several mercury monitoring programs, including the Global Mercury Observing System (GMOS), the Arctic Monitoring and Assessment Programme (AMAP), and the North American Mercury Deposition Network (NAMDN), have been initiated worldwide. Despite the international regulations and directives enforcing stringent restrictions on the use and sale of mercury-containing products, activities such as mining, the paint industry, the paper and pulp industry, the chloro-alkali industry, coal burning, power plants, the incineration of waste, and oceanic and volcanic emissions are the major sources of mercury pollution.[2,7]

Different methodologies have been developed and applied for the water and wastewater treatment. These include screening, centrifugation, microfiltration and ultrafiltration, crystallization, sedimentation/gravity separation, flotation, precipitation, coagulation, oxidation, solvent extraction, evaporation, distillation, reverse osmosis, ion exchange, electrodialysis, electrolysis, adsorption, etc. In comparison to others, adsorption is considered to be simple, attractive, and the most suitable process for the extraction of toxic metals from water, because of the ease of operation, cost-effectiveness, and availability of a wide range of adsorbents.[8,9] In recent years, the idea of designing nanoparticle surfaces displaying improved adsorbate uptake capacity has raised broad scientific and technological interest. This interest is further augmented by the provision of covalently anchoring various functional groups at the surface of nanoparticles (NPs). NPs are of great interest in water treatment, because of their high surface-to-volume ratio, which leads to a higher uptake capacity.[10−13] Among the various nanomaterials under investigation, the magnetic nanoparticles (MNPs) have been attracting particular attention, because of their convenient magnetic field-assisted separation.[14−16]

Chelating functionalities such as amine, thiol, thiocarbamate, carbonyl, and phosphoryl moieties on the surface of a solid support have gained significant attention for the removal of heavy-metal ions from their aqueous solutions.[17] These organic chelating ligands can form strong complexes with various metal ions. For example, Hg^{II} ions have a distinct affinity to bind strongly with the sulfur-containing functional groups[18] and, hence, can be effectively trapped from the water by employing sulfur-containing chelating agents such as thiol, dithiocarbamate (DTC), 1-(2-thiazolylazo)-2-naphthol, mercaptopropylsilane, 1-furoyl thiourea, benzoylthiourea, and mercaptobenzothiazole.[19,20] These functional groups have been previously attached to the surface of a variety of nanomaterials, e.g., mesoporous silica, activated carbon, and organoceramic composites.[19,21−23] Among MNPs, magnetite (Fe_3O_4) NPs have been widely investigated to study the removal of dyes, harmful microorganisms, and toxic heavy metals (such as Pb, Hg, As, Cd, and Cr) from water.[9,24−26] Both covalent and noncovalent surface functionalization strategies have been exploited to appropriately functionalize the surface of MNPs with metal-ion chelating groups. The noncovalent architectures are easy to fabricate. However, they are prone to disassemble and, hence, exhibit poor long-term chemical stability.[27−32] Although the covalent strategies are chemically more robust, but they have not been explored to their full potential. The covalent strategies have generally been limited to monolayer-based surface modifications, where only one ion-exchanging or chelating functionality per anchoring molecule is incorporated at the surface of MNPs,[24,33,34] thus providing limited surface functional group density. In contrast, surface-anchored polymer chains (polymer brushes) provide a very convenient means of increasing the surface functional group density.[35,36] Polymer brushes have undergone enormous development, offering vast synthetic flexibility toward the introduction of a variety of functional groups at the surface of a range of materials.[37] In context of water remediation application, this platform offers a convenient means of increasing the pollutant uptake capacity of an adsorbent such as MNPs.

In order to prove this hypothesis, we are capitalizing on a recent report from Girginova et al.,[34] in which they have evaluated the potential of dithiocarbamate-derivatized silica-coated MNPs for the removal of Hg^{II} ions from water. They reported an uptake efficiency of 74% for monolayer-based DTC-functionalized MNPs, compared to 24% for MNPs without DTC, at a contamination level of 50 $\mu g\ L^{-1}$.[34] Considering this as a reference material, we have synthesized novel polymer-grafted MNPs containing pendant dithiocarbamate functional groups. Although the polymer coating on MNPs may reduce their magnetic properties, materials with optimum properties suitable for a particular application can be achieved by controlling the amount of polymer coating the surface.[24] Surface-initiated conventional radical polymerization (SI-cRP), by using an azo-initiator immobilized on the amine-functionalized magnetite nanoparticles (MNPs-NH_2), was employed for the growth of covalently bonded chains of 2-aminoethyl methacrylate hydrochloride (AEMA·HCl) polymer from the surface of MNPs. Finally, the reaction of these polymer-grafted-MNPs with CS_2 in basic medium resulted in the conversion of pendant $-NH_2$ groups of the surface-grafted polyAEMA·HCl to the DTC groups. We have compared the Hg^{II} ion removal capacity of MNPs-DTC and MNPs-polyAEMA·DTC, which proved that the polymer-grafted MNPs exhibit higher removal capacity. The ultimate objective of this study was to demonstrate the impact of surface functional group density of the DTC chelating groups on the Hg^{II} ions uptake capacity of MNPs from contaminated water.

EXPERIMENTAL SECTION

Materials. Ferrous sulfate heptahydrate ($FeSO_4·7H_2O$, 99%), potassium nitrate (KOH, 99%), (3-aminopropyl) triethoxysilane (APTES) (98%), tetraethylorthosilicate (TEOS) (99%), methanol (>98.5%), dry dichloromethane, sodium chloride (99%), 4,4′-azobis (4-cyanopentanoic acid) (98.0%), triethylamine (TEA) (99%), and 2-aminoethyl methacrylate hydrochloride (AEMA·HCl) (90%) were used as received from Sigma−Aldrich, Germany. Mercuric nitrate 95% was obtained from Merck, Germany. Sodium hydroxide (98%) was obtained from Fisher Scientific, USA. Aqueous ammonia solution 35% was obtained from BDH AnalaR, U.K. Carbon disulfide (98%), potassium hydroxide (98%), and toluene (99%) were purchased from Riedel-de Haën, Germany. Toluene was dried using Na/benzophenone prior to use. TEA was refluxed overnight with calcium hydride, distilled, and stored under a nitrogen atmosphere. 4,4′-Azobis(4-cyanopentanoyl chloride) (ACPC) was synthesized from 4,4′-azobis (4-cyanopentanoic acid) according to a previously reported method.[38]

Methods. *Synthesis of Monolayer-Based DTC-Grafted MNPs (MNPs-DTC).* The monolayer-based DTC-grafted magnetic nano-

particles (MNPs-DTC) were synthesized using the method previously reported by Girginova et al.[34] MNPs were obtained via the basic hydrolysis of an iron (Fe^{II}) salt. Briefly, $FeSO_4{\cdot}7H_2O$ (20.0 g, 74 mmol) was dissolved in 140 mL of water, and a solution of KNO_3 (1.62 g, 16 mmol) and KOH (11.23 g, 0.20 mol) in 60 mL H_2O was added dropwise to it under nitrogen bubbling. The black precipitates obtained were mechanically stirred for an additional 1 h at 90 °C and left overnight at room temperature (rt). The formed magnetite (Fe_3O_4) particles were washed several times with deionized water and separated using a permanent magnet. Transmission electron microscopy (TEM) of the pristine MNPs (Figure 1) showed a

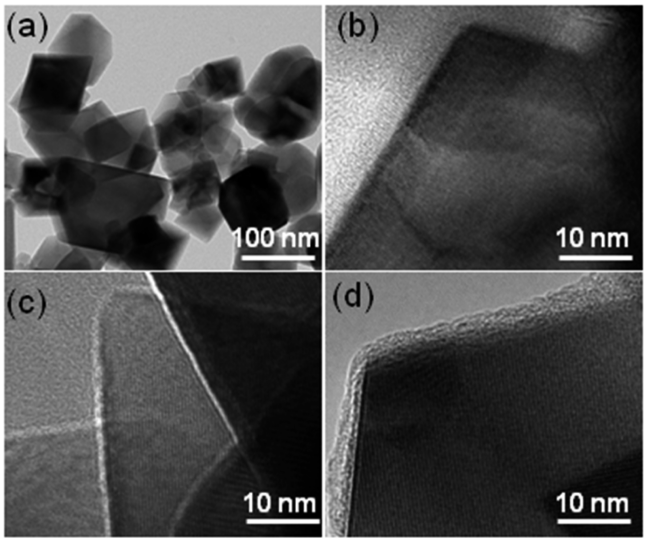

Figure 1. Transmission electron microscopy (TEM) image of (a) as-prepared Fe_3O_4 MNPs, (b) zoomed-in edge of as-prepared MNPs, (c) APTES-derived monolayer-based DTC-functionalized MNPs (MNPs-DTC), and (d) polyAEMA·HCl polymer-brush-based DTC-functionalized MNPs (MNPs-polyAEMA·DTC).

predominantly polydisperse multifaceted morphology with a wide particle size distribution. The silica-coated MNPs (MNPs-TEOS) were prepared by sonicating the MNPs (250 mg) in ethanol (188 mL), followed by the addition of ammonia solution (15 mL, 35%) and TEOS (0.5 mL, 2.24 mmol). The suspension was further sonicated for 2 h in an ice bath and the prepared particles were washed thoroughly with ethanol and collected by using an external permanent magnet. The amine-functionalized MNPs (MNPs-APTES) were synthesized by dispersing the MNPs-TEOS (250 mg) into 83 mL of 2% APTES (v/v) solution in ethanol. The suspension was mechanically stirred for 3 h at 40 °C, the obtained APTES-coated particles were washed with ethanol and finally collected magnetically. The DTC-functionalized particles were obtained by dispersing APTES-modified MNPs (100 mg) in a mixture of aqueous NaOH solution (318 mL, 0.1 M), 2-propanol (63 mL), and CS_2 (4.8 mL, 0.07 mol), followed by mechanical stirring for 6 h at rt. The DTC-grafted MNPs (MNPs-DTC) were separated with the help of a permanent magnet, washed thoroughly with 2-propanol, and dried at rt.

Immobilization of Azo-initiator on the Surface of Aminated MNPs (MNPs-AI). A solution of azo-initiator was prepared by dissolving ACPC (0.6 g, 2.8 mmol) in 20 mL of dry dichloromethane, followed by the addition of dry TEA (260 μL, 1.87 mmol) under nitrogen gas (N_2). This solution was injected over predegassed APTES functionalized MNPs (MNPs-APTES 0.6 g) under N_2(g) atmosphere. The particles were shaked on an orbital shaker for 2.5 h at rt, followed by washing with dichloromethane (2 × 30 mL) and methanol (2 × 30 mL) and finally separation via permanent magnet. The particles obtained will, hereafter, be designated as MNPs-AI.

Synthesis of polyAEMA·HCl-Functionalized MNPs (MNPs-polyAEMA·HCl). AEMA·HCl monomer (2 g, 12.08 mmol) was dissolved in 10 mL of deionized water and solution was degassed by nitrogen gas bubbling for 1 h. The mixture was injected into already-degassed MNPs-AI and allowed to polymerize for 6 h at 65 °C. The polymerization was quenched by exposing the reaction mixture to air. The poly(AEMA·HCl)-functionalized MNPs (MNPs-polyAEMA·HCl) were purified by subjecting them several times to sonication and washing with deionized water. The prepared MNPs-polyAEMA·HCl were separated by employing a permanent magnet and dried at rt under ambient pressure.

Transformation of Amine Groups of MNPs-polyAEMA to DTC Groups (MNPs-polyAEMA·DTC). MNPs-polyAEMA (200 mg) was dispersed in a mixture of aqueous NaOH solution (630 mL, 0.1 M), 2-propanol (126 mL), and CS_2 (9.5 mL, 0.152 mol). The suspension was mechanically stirred for 6 h at room temperature. The DTC-functionalized MNPs-polyAEMA (MNPs-polyAEMA·DTC) was collected magnetically from the suspension, washed thoroughly with 2-propanol, and dried at rt.

Characterization. Attenuated total reflectance−infrared (ATR-IR) spectra were recorded on the samples, using a Nicolet Model FT-IR 730 spectrometer. For each sample, 1000 scans were taken at a resolution of 4 cm^{-1} with an induction time of 20 min for N_2 exposure (to eliminate noise from atmospheric water). Omnic series software was utilized for data acquisition. TEM images were obtained by using FEI Tecnai G2 F30 instrument. Samples were prepared by drop casting two to three drops of particle dispersions in ethanol onto carbon-coated copper TEM grids. X-ray photoelectron microscopy (XPS) measurements were carried out using Thermo Scientific K-Alpha equipment. The Mg Kα (1253.6 eV) X-ray source was operated at 300 W. A pass energy of 117.40 eV was used for the survey spectra. The spectra were recorded using a 60° takeoff angle, relative to the surface normal. A Physical Property Measurement System (PPMS) device (Cryogenic, 12 T Magnet) was used to measure magnetic properties of MNPs. Thermogravimetric analysis (TGA) was performed with a TA Instruments device (Model TGA Q500) from rt to 1000 °C at a heating rate of 10 °C/min under a nitrogen gas (N_2) atmosphere (40 mL/min).

Mercury Uptake Studies. The Hg^{II} uptake capacity of MNPs-DTC and MNPs-polyAEMA·DTC particles was studied by using various amounts of adsorbents. Functionalized particles (5−20 mg) were added to 10 ppm Hg^{II} solution (10 mL) and stirred at room temperature for 12 h. Particles were then separated with a permanent magnet, and the supernatant was treated with dithizone solution (0.001% in $CHCl_3$) to obtain a stable orange-colored complex.[39] The organic layer was washed with 20% aqueous NH_3 solution (20 mL × 3), followed by washing with 12% aqueous acetic acid (20 mL × 2) and finally with Milli-Q water (20 mL × 2). Then, the organic layer was transferred to a volumetric flask (25 mL) and filled up to the mark with chloroform. Finally, the Hg^{II} concentration was measured by an ultraviolet-visible light (UV/Vis) spectrophotometer at 490 nm using the calibration curve as depicted in Figure S1 in the Supporting Information.

$$\text{Hg}^{\text{II}}\text{ ion removal efficiency (\%)} = \frac{C_1 - C_2}{C_1} \times 100 \quad (1)$$

where C_1 is the concentration of Hg^{II} ions in water before treatment with magnetic adsorbent and C_2 is the concentration of Hg^{II} ions in water after treatment with magnetic adsorbent. The effect of contact time and temperature on removal capacity was carried out in the same manner with 10 mg particles, using 10 ppm Hg^{II} solution. All the Hg(II) uptake experiments were performed at neutral pH.

RESULTS AND DISCUSSION

Synthesis of Monolayer- and Polymer-Brush-Based DTC-Functionalized MNPs. Monolayer-based DTC-functionalized MNPs (MNPs-DTC) were prepared according to a reported procedure.[34] This included the synthesis of MNPs using a precipitation method that employs the hydrolysis of ferrous sulfate in a basic medium. In the next step, MNPs were

Scheme 1. Schematic Illustration of the Synthesis of Monolayer (MNPs-DTC) and Polymer Brush (MNPs-polyAEMA·DTC)-Based DTC-Functionalized MNPs

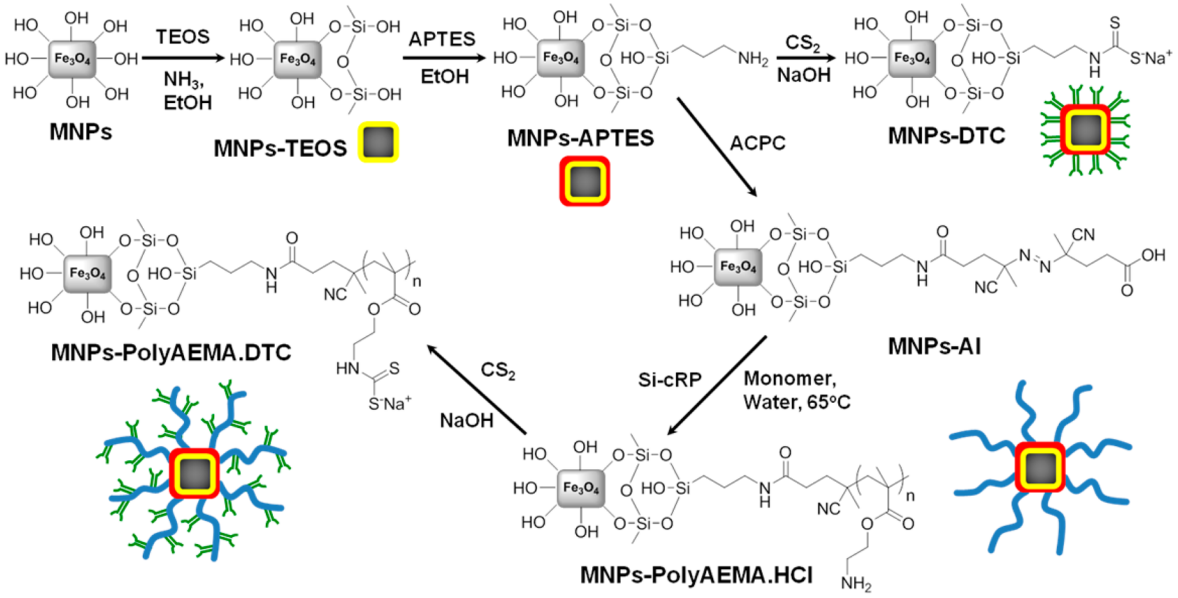

functionalized with a thin silica layer, using TEOS, followed by the treatment with APTES, which resulted in the synthesis of amine-functionalized MNPs. The reaction of surface amino groups with CS_2 in an alkaline medium lead to the formation of MNPs-DTC. For the synthesis of polymer-brush-based DTC-functionalized MNPs (MNPs-polyAEMA·DTC), MNPs-APTES bearing surface amino groups, from the same batch as those prepared for MNPs-DTC, were functionalized with an azo initiator to provide sites for the surface-initiated free-radical polymerization. The azo initiator was grafted on aminated nanoparticles in dry DCM under inert atmosphere in the presence of dry TEA through amide bond formation between surface $-NH_2$ groups and acid chloride groups of ACPC. Surface-initiated conventional radical polymerization (SI-cRP) was thermally initiated from the surface of AI-MNPs in the presence of the AEMA·HCl monomer under inert atmosphere. This resulted in polyAEMA·HCl chains covalently bound at the surface of MNPs. The complete synthesis pathway is summarized in Scheme 1.

Characterization of the Functionalized MNPs. The TEM investigation revealed that the synthesized MNPs have mainly sharp and well-defined clean edges, and the average particle size was ~80 nm (see Figures 1a and 1b). The sharp edges may have originated from the anisotropic growth mechanism; Girginova et al.[34] have also reported analogous particle morphology under similar MNPs synthesis conditions. Functionalization with TEOS and APTES resulted in the appearance of a very thin layer at the surface of MNPs (Figure 1c), whereas the grafting of polyAEMA·HCl chains resulted in the appearance of a much thicker layer (~5 nm) uniformly covering the entire surface of MNPs (Figure 1d). The TEM images thus corroborated the higher amount of material deposited on particles surface via polymer-brush-based surface functionalization in comparison to monolayer based strategy.

The higher amount of organic content incorporated at the surface of MNPs-polyAEMA·DTC was further evident from the TGA analysis (Figure 2). The MNPs-DTC showed ~1% weight loss, whereas MNPs-polyAEMA·DTC showed a significantly higher weight loss (~5%) at 450 °C. Considering

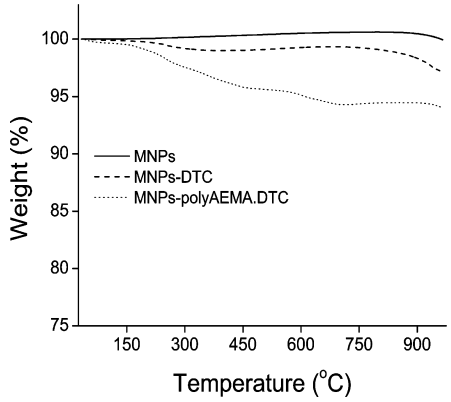

Figure 2. TGA thermograms of as-prepared MNPs, MNPs-DTC, and MNPs-polyAEMA·DTC.

the molecular structures of the monolayer used in the present studies (we have not included silicon, because we believe that silicon will remain in the ashes in the form of silicon oxide), the weight loss in TGA reflected that for each 100 g of MNPs-DTC, the amount of DTC chelating functionality incorporated at the surface was 0.0064 mol. Under the same assumptions, the weight loss in TGA reflected that, in the case of MNPs-polyAEMA·DTC, the amount of DTC chelating functionality incorporated at the surface was 0.022 mol. This analysis showed a substantially higher surface functional group density for MNPs-polyAEMA·DTC and supported the observations made in the TEM investigation.

After confirming the different amounts of material deposited at the surface of MNPs-DTC and MNPs-polyAEMA·DTC, the effect of surface coverage on the magnetization of these particles were tested under the applied magnetic field. The extent of magnetization of MNPs in response to the applied magnetic field is affected by the shielding effect of the surface coating.[40] Thicker coatings generally result in higher shielding, which leads to lower magnetization in the applied magnetic field. In the present study, the magnetic measurements of bare and functionalized MNPs were carried out at 298 K employing

PPMS. The magnetization versus applied magnetic field curves depicted in Figure 3 clearly indicate a difference in the magnetic

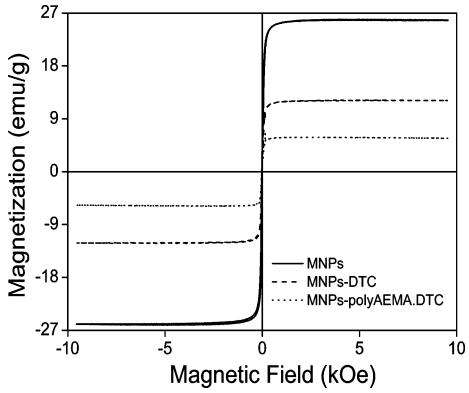

Figure 3. Room-temperature (298 K) magnetization curves for as prepared MNPs, MNPs-DTC, and MNPs-polyAEMA·DTC.

properties of particles after surface modification. Bare MNPs showed the highest magnetization which was decreased after the surface functionalization as in case of MNPs-DTC and MNPs-polyAEMA·DTC showed the lowest magnetization in response to the applied magnetic field. This observation is in accord with the observations reported in the literature, regarding the decrease in magnetization for thicker surface coatings.[41] The thicker polymer layer, as observed in TEM images, and higher grafting density as estimated from TGA (Figures 1 and 2), offered higher shielding compared to the monolayer. However, the polymer-functionalized MNPs were sufficiently magnetic and could be readily separated from the water solutions of Hg(II) by employing a permanent magnet (refer to the video provided in the Supporting Information). Since we used mild experimental conditions for Fe_3O_4 MNPs synthesis followed by a stepwise coating of the Fe_3O_4 MNPs with silica shell employing TEOS, APTES, an initiator, and subsequent functionalization with polymer, we believe that the decrease in magnetization is due to the shielding caused by the layers coating the MNPs surface during the functionalization process. The Fe_3O_4 MNPs were already coated with silica shell and APTES before they were brought into contact with CS_2. At this stage, the particles clearly showed a decrease in the magnetization, which excludes the contribution to magnetization loss from the loss of surface iron atoms by Fe−S chelation.[24,34,40,41]

The important characterization data for the MNPs are collated in Table 1.

The incorporation of monolayer- and polymer-brush-based DTC chemical functionalities at the surface of MNPs was successfully ascertained by ATR-IR spectroscopy. The region of interest for the ATR-IR spectra is depicted in Figure 4. For

Table 1. MNPs Characterization Data

MNPs	size (nm)[a]	shape	amount of chelating functionality (mol/100 g of MNPs)[b]
pristine MNPs	80	multifaceted	
MNPs-DTC			0.0064
MNPs-polyAEMA·DTC			0.022

[a]Average particle size from TEM. [b]Estimated from TGA.

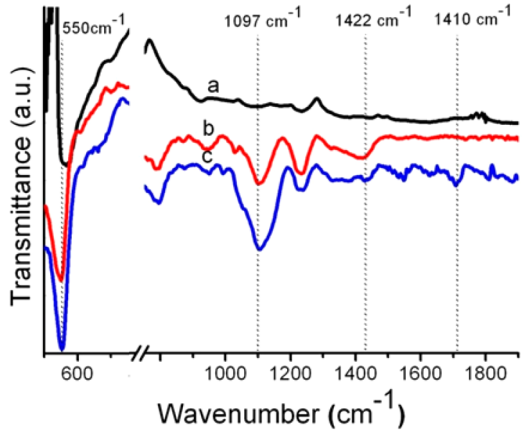

Figure 4. ATR-IR spectra of (a) pristine Fe_3O_4 MNPs, (b) MNPs-DTC, and (c) MNPs-polyAEMA·DTC.

pristine Fe_3O_4 MNPs, the characteristic (Fe−O) vibrational band appeared at ∼550 cm^{-1}. Surface modification of MNPs with APTES-derived monolayer-based DTC was confirmed by the appearance of Si−O−Si stretching vibration at 1097 cm^{-1}, which showed the successful TEOS and APTES functionalization. The signal for DTC groups at 1422 cm^{-1} established the successful transformation of amino groups to DTC groups.[34,42] Similar to MNPs-DTC, MNPs-polyAEMA·DTC also showed the characteristic signals for Si−O−Si and DTC groups. In addition, the characteristic signal for carbonyl stretching vibration was observed at 1710 cm^{-1} in the case of polymer-brush-functionalized MNPs.

The chemical nature of the surface coatings and hence the success of the surface modifications was further established by XPS analysis (Figure 5). The binding energies of Fe $2p_{1/2}$ and Fe $2p_{3/2}$ at 725 and 711 eV were totally in agreement with Fe_3O_4, instead of Fe_2O_3.[43] Surface modification of MNPs with APTES resulted in the appearance of signal for nitrogen (N 1s) at 400 eV indicating successful functionalization of MNPs surface with amino groups. The associated signals for silicon appeared at 153 and 103 eV for Si 2s and Si 2p, respectively. The C 1s signal for the carbon content incorporated on the surface appeared at 285 eV, which further confirmed the successful functionalization of MNPs with APTES (Figure 5a). The subsequent transformation of surface amino groups to DTC groups was confirmed by the appearance of the S 2s (233 eV) and S 2p (169 eV) signals for sulfur (Figure 5b). In the case of MNPs-polyAEMA·HCl, the XPS survey scan showed the signal for Cl 2s (268 eV) and Cl 2p (198 eV), because of the chlorine incorporated on the surface as the monomer used for the polymer brush growth was in its hydrochloride form (Figure 5c). Similar to the monolayer-based surface functionalization, the transformation of surface amino groups to DTC groups was confirmed by the appearance of S 2s (233 eV) and S 2p (169 eV) signals for sulfur incorporated on the surface of MNPs (Figure 5d). Furthermore, since the polymer brushes result in a high density of surface functional groups, consequently, a higher percentage of sulfur (surface atomic concentration = 4.9%) was observed for MNPs-polyAEMA·DTC, compared to MNPs-DTC (surface atomic concentration = 1.9%). This observation is in accord with the TEM, TGA, and PPMS investigations and confirmed the higher surface functional group density in case of MNPs-polyAEMA·DTC. The auger signal for Na in both cases further

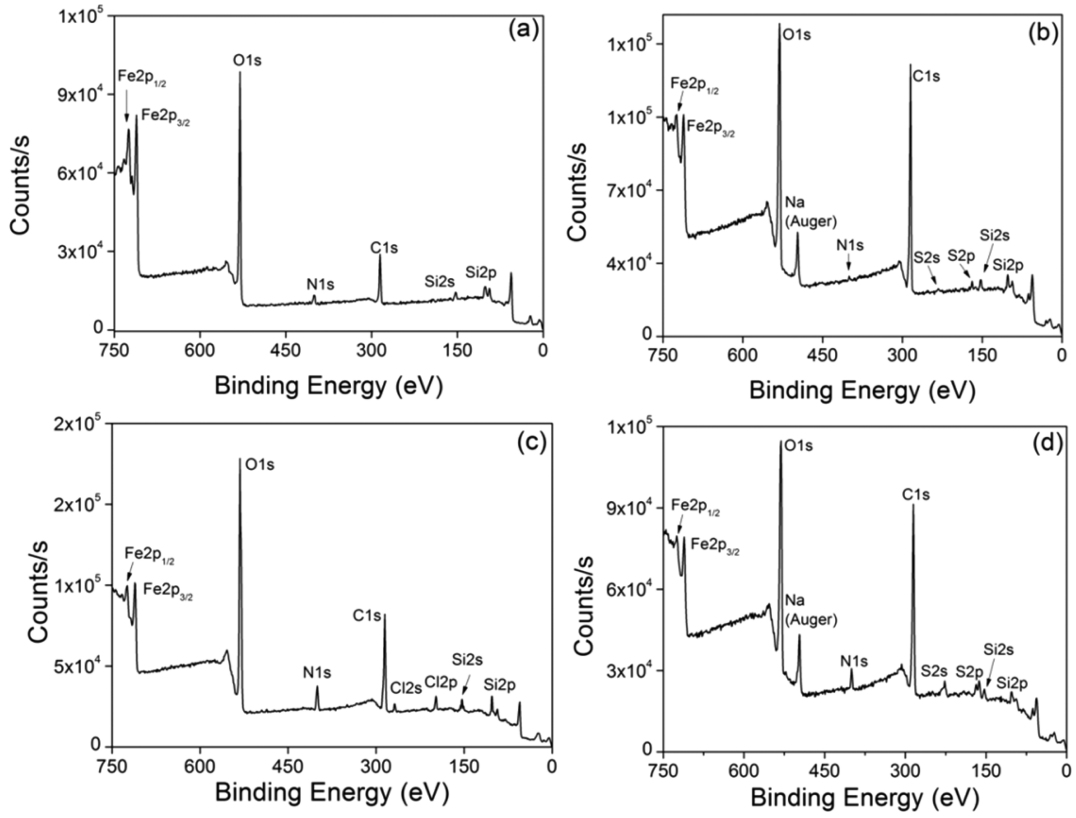

Figure 5. XPS survey scans: (a) MNPs-APTES, (b) MNPs-DTC, (c) MNPs-polyAEMA·HCl, and (d) MNPs-polyAEMA·DTC.

confirmed the presence of sodium salt of DTC moieties at the surface of MNPs (Figures 5b and 5d).

Effect of Adsorbent Amount on Hg^{II} Removal. The investigation of adsorption capacity was carried out at rt for varying amounts of particles (5, 10, 15, and 20 mg). For the sake of comparison, the fix amounts of MNPs-DTC and MNPs-polyAEMA·DTC were separately added to 10 mL of a 10 ppm Hg^{II} solution and the suspensions were shaken on an orbital shaker at room temperature for 12 h. The change in Hg^{II} uptake with varying amount of MNPs-DTC and MNPs-polyAEMA·DTC showed that there is an increase in the adsorption with an increase in the amount of adsorbent (Figure 6).[44,45]

In order to demonstrate the Hg^{II} removal associated with the DTC groups, we also performed the uptake experiments with the MNPs functionalized with monolayer- and polymer-brush-based amine functional groups (MNPs-APTES and MNPs-polyAEMA). The APTES-functionalized MNPs showed lower uptake capacity. Twenty milligrams (20 mg) of MNPs-APTES could only remove 13% of Hg^{II} from a 10 ppm solution of Hg^{II}. After the transformation of surface amine groups to DTC groups, the 20 mg of MNPs-DTC removed 72% of the Hg^{II} species from the 10 ppm Hg^{II} solution. In the case of MNPs-polyAEMA, we observed a surprisingly high Hg^{II} (93%) removal from the 10 ppm solution. We attribute this superior percentage removal capacity of MNPs-polyAEMA to the higher surface functional group density of amino groups and to the pendent ester linkages, which are available only in polyAEMA brush and not in the case of monolayer. The Hg^{II} ions can be chelated by both the amino groups and ester linkages. This led to an unexpectedly higher Hg^{II} removal capacity of MNPs-polyAEMA in comparison with the MNPs-APTES. Among all

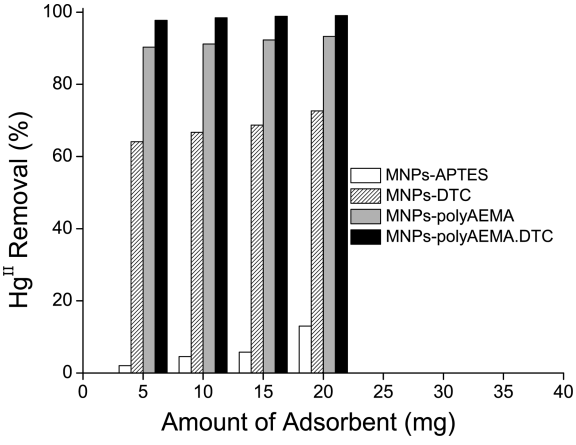

Figure 6. Comparison of Hg^{II} ion removal capacity for different amounts (5−20 mg) of MNPs-APTES, MNPs-DTC, MNPs-polyAEMA, and MNPs-polyAEMA·DTC. The given amount of the adsorbent was added to 10 mL of a 10 ppm Hg^{II} solution in water and incubated for 12 h.

MNPs, MNPs-polyAEMA·DTC exhibited the highest percentage of Hg^{II} removal. Even for 5 mg of the MNPs-polyAEMA·DTC, the removal percentage was 97%, which reached to almost-complete removal when 20 mg of the MNPs-polyAEMA·DTC were added to the 10 ppm solution of Hg^{II} ions. Figure 7 displays the comparison of percentage removal capacity of MNPs-DTC and MNPs-polyAEMA·DTC. Further studies were performed with 10 mg particles, using a 10 ppm Hg^{II} solution.

Effect of Contact Time on Hg^{II} Removal. In order to determine the optimum time necessary for the best uptake

dx.doi.org/10.1021/am400427n | ACS Appl. Mater. Interfaces 2013, 5, 3784−3793

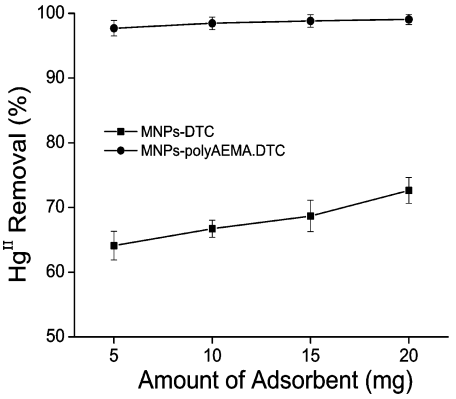

Figure 7. A comparison of Hg^{II} ions removal capacity for different amounts of MNPs-DTC and MNPs-polyAEMA·DTC. The given amount of each type of adsorbent was added to 10 mL of 10 ppm Hg^{II} ions solution in water and incubated for 12 h.

efficiency, the effect of MNPs contact time on Hg^{II} removal percentage of developed MNPs was studied. The DTC-functionalized MNPs (10 mg) were added to the 10 ppm Hg^{II} solution for time periods ranging from 6 h to 56 h, with a 6 h increment interval. MNPs-polyAEMA·DTC exhibited an almost-complete removal of Hg^{II} from the 10 ppm solution after 24 h, whereas for MNPs-DTC, the percentage removal after 24 h was ∼68% under the similar conditions. Ten milligrams (10 mg) of MNPs-DTC could show a maximum Hg^{II} removal of 77% from the 10 ppm Hg^{II} solution after 56 h of contact time (Figure 8). This was the maximum removal that

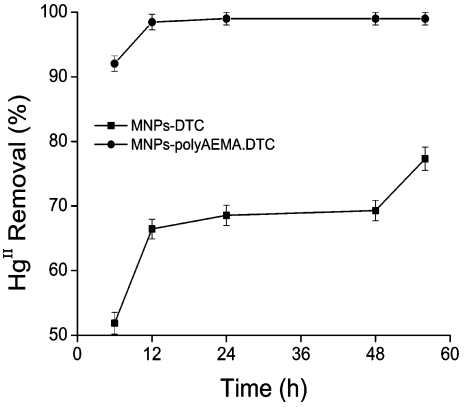

Figure 8. Effect of contact time on the removal capacities of MNPs-DTC and MNPs-polyAEMA·DTC. The comparison depicted here is for 10 mg of each type of MNPs added to 10 mL of a 10 ppm Hg^{II} ions solution in water.

could be achieved for monolayer-based DTC-functionalized MNPs under these conditions and any further increase in the contact time did not increase the percentage removal, reflecting on the limit of adsorption capacity of MNPs-DTC. This clearly indicated superior Hg^{II} uptake characteristics of polymer-grafted MNPs, compared to monolayer functionalized ones. These results showed that the MNPs-polyAEMA·DTC not only display high removal capacity but they also possess high removal efficiency, compared to the MNPs-DTC. We attribute the higher removal capacity and efficiency of MNPs-polyAEMA·DTC to the higher surface functional group density of the adsorption sites.[44,46]

Effect of Temperature on Hg^{II} removal. Influence of temperature on adsorption efficiency was investigated at various temperatures (30, 40, 50, and 60 °C). For each temperature point, 10 mg of both types of DTC-functionalized MNPs were added to 10 mL of a 10 ppm Hg (II) solution and the suspensions were shaken for 12 h. The removal tendency of the adsorbents generally increases as the temperature increases.[45−47] In the case of MNPs-polyAEMA·DTC, the increase in the removal capacity may not be very striking, as the uptake capacity is extremely high, even at room temperature. However, the Hg^{II} removal capacity of MNPs-DTC increased sharply from 30 °C to 40 °C, and beyond 40 °C, it increased at a slower pace. It reached its maximum value of 83% at 60 °C (Figure 9). This prominent increase in the

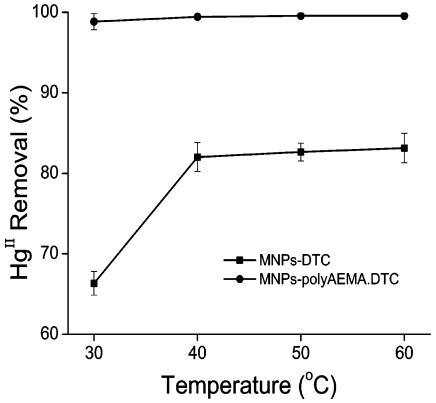

Figure 9. Effect of temperature on removal capacity of MNPs-DTC and MNPs-polyAEMA·DTC. The comparison depicted here is for 10 mg of each type of MNPs added to 10 mL of a 10 ppm Hg^{II} ion solution in water.

removal capacity may be attributed to the better dispersion of MNPs-DTC at higher temperature. A 100% removal of Hg^{II} at 40 °C by MNPs-polyAEMA·DTC highlights their superior removal characteristics over MNPs-DTC.

These uptake studies demonstrate the scope of polymer brushes as facile means of enhancing surface functional group density in the context of environmental remediation. The number of chelating sites at the surface may not be a limiting factor for 100% removal of the contaminants; however, the higher surface functional group density certainly offers the advantage of higher removal efficiency, along with higher removal capacity (refer to Figures 7 and 8). This implies that a smaller amount of adsorbent is required that can perform the remediation process in a shorter period of time, thus saving material as well as time. For the proof of concept, we have used Hg(II)/DTC-functionalized MNPs as a model adsorbate/adsorbent system and the developed concept can be extended to other adsorbates.

Approximation of Adsorption Behavior. The adsorption isotherm was used to evaluate the adsorption properties of the adsorbent at rt, which is important for understanding the mechanism of the adsorption. The relationship between adsorbent and adsorbate was established by applying the Langmuir and Freundlich models. These isotherms not only explain adsorption capacity but also give insight about surface properties and adsorbent/adsorbate affinity constants.[22,23]

The Langmuir isotherm explains adsorption on specific adsorbent sites. In this model, adsorbate moieties (Hg^{II}) are assumed to undergo a monolayer type adsorption, depending

on the active sites on adsorbent surface (MNPs).[48] The parameters of Langmuir isotherm are established by the following relation:

$$\frac{C_e}{q_e} = \frac{1}{q_{max} b} + \frac{C_e}{q_{max}} \quad (2)$$

where C_e is the equilibrium concentration of adsorbate entities in the solution (mg L^{-1}), q_e defines the amount of adsorbate entities adsorbed on the unit amount of the adsorbent at equilibrium (mg g^{-1}), q_{max} (mg g^{-1}) represents the maximum adsorption capacity of adsorbent, and b (L mg^{-1}) is defined as the affinity of binding sites or the Langmuir constant.

The maximum adsorption capacities of MNPs-DTC and MNPs-polyAEMA·DTC for Hg^{II} adsorbate ions were calculated as 47.870 ± 0.110 mg g^{-1} and 59.453 ± 0.320 mg g^{-1}, respectively (see Table 2). (Also see Figure S2 in the Supporting Information.) This showed that the adsorption capacity of MNPs-polyAEMA·DTC is higher than MNPs-DTC. Furthermore, the Langmuir constant (b) for MNPs-polyAEMA·DTC (0.3537 ± 0.036 L mg^{-1}) is 1 order of magnitude higher than MNPs-DTC (0.031 ± 0.002 L mg^{-1}). The higher b value indicates a stronger attraction of Hg^{II} ions on the MNPs-polyAEMA·DTC surface, compared to the MNPs-DTC adsorbent surface.

Table 2. Adsorption Behavior of MNPs-DTC and MNPs-polyAEMA·DTC Approximated by Langmuir and Freundlich Isotherm Models (the Associated Calculated Parameters Are Enlisted)

parameter	Value: MNPs-DTC	Value: MNPs-polyAEMA·DTC
Langmuir Model		
q_{max} (mg g^{-1})	47.870 ± 0.110	59.453 ± 0.320
b (L mg^{-1})	0.031 ± 0.002	0.3537 ± 0.036
R_L	0.3937	0.0535
R^2	0.9789	0.9428
Freundlich Model		
K_f	1.969 ± 0.114	20.172 ± 0.308
$1/n$	0.8226	0.0469
R^2	0.9543	0.9685

The separation factor, or equilibrium parameter (R_L), which is a dimensionless constant generally used to express the feasibility of the adsorption. The values of $1 > R_L > 0$, $R_L > 1$, and $R_L = 0$ indicate a favorable, unfavorable, and irreversible interactions, respectively. The R_L values are calculated using the following equation:

$$R_L = \frac{1}{bC_0 + 1} \quad (3)$$

where C_0 is the initial concentration of adsorbate entity (mg L^{-1}) and, in the present study, C_0 = 50 mg L^{-1}. Accordingly, the calculated R_L values were in the range of $0 < R_L < 1$, indicating a favorable adsorption of Hg^{II} by both MNPs-DTC (R_L = 0.3937) and MNPs-polyAEMA·DTC (R_L = 0.0535).

The Freundlich adsorption isotherm relates adsorption capacity and intensity based on concentration of an adsorbate on adsorbent to its concentration in solution.[48] Besides, this isotherm model considers the heterogeneous surface adsorption. The linear form of Freundlich isotherm can be written as follows:

$$\log q_e = \log K_f + \frac{1}{n} \log C_e \quad (4)$$

where K_f is the uptake factor and $1/n$ represents the heterogeneity or Freundlich's intensity factor. The value of $1/n$ is important, since it approximately gives information about the ease of adsorption. A value of $1/n$ in the range of $0.1 < 1/n < 1.0$ indicates highly favorable adsorption; a value of $1/n > 2$ will lead to an unfavorable adsorption. This parameter $(1/n)$ was calculated as 0.8226 and 0.0469 for MNPs-DTC and MNPs-polyAEMA·DTC, respectively (see Figure S3 in the Supporting Information). This indicated a more favorable adsorption process for MNPs-polyAEMA·DTC, since smaller values of $1/n$ show better interaction for adsorption.

A comparison of the two isotherms based on the linear regression coefficient (R^2) values (Table 1) showed that the Hg^{II} adsorption on MNPs-DTC is better estimated by the Langmuir isotherm (R^2 = 0.9789). However, the Hg^{II} adsorption on MNPs-polyAEMA·DTC conforms Freundlich isotherm (R^2 = 0.9685), under the concentration range studied.

Adsorption Kinetics. Kinetics of adsorption is used to study adsorption rate and pathways of adsorption until equilibrium is reached. Rate of adsorption in the present study was determined by using different rate equations. Pseudo-first-order and pseudo-second-order mechanisms were investigated for determining adsorption kinetics. The comparison was then drawn between the experimental and calculated data. The following Lagragrian rate equations describe pseudo-first-order and pseudo-second-order models:[46,49−51]

Pseudo-first-order:

$$\log(q_e - q_t) = \log q_e - \left(\frac{k_1}{2.303}\right) t \quad (5)$$

Pseudo-second-order:

$$\frac{t}{q_t} = \frac{1}{k_2 q_e^2} + \frac{1}{q_e} t \quad (6)$$

where q_e (mg/g) is the amount of Hg^{II} adsorbed per unit mass of adsorbent at equilibrium and q_t (mg/g) is the Hg^{II} adsorbed at time t, while k_1 (min^{-1}) and k_2 (g/mg min^{-1}) are equilibrium rate constants of pseudo-first-order and pseudo-second-order adsorption interactions, respectively.

The kinetic rate constants and correlation coefficient (R^2) of both models are summarized in Table 3. According to these results, the kinetic behavior is well-described by a pseudo-

Table 3. Kinetic Parameters Associated with the Adsorption of Hg^{II} Ions with MNPs-DTC and MNPs-polyAEMA·DTC

parameter	MNPs-DTC	MNPs-polyAEMA·DTC
Pseudo-First-Order Kinetics		
q_e (mg g^{-1})		
experimental	8.202	9.907
calculated	3.006	0.863
k_1 (min^{-1})	3.901×10^{-3}	2.742×10^{-3}
R^2	0.874	0.692
Pseudo-Second-Order Kinetics		
q_e (mg g^{-1})		
experimental	8.202	9.907
calculated	7.932	9.619
c_2 (min^{-1})	5.510×10^{-4}	3.712×10^{-3}
R^2	0.993	0.998

dx.doi.org/10.1021/am400427n | ACS Appl. Mater. Interfaces 2013, 5, 3784−3793

second-order mechanism that provided the best value of R^2. It is calculated as 0.993 and 0.998 for MNPs-DTC and MNPs-polyAEMA·DTC, respectively (see Figure S4 in the Supporting Information). Similarly, a reasonable agreement between the calculated and experimental values of q_e is a good indication of favorable adsorption kinetic order. The corresponding equilibrium rate constant (k_2) for MNPs-polyAEMA·DTC was an order of magnitude higher than MNPs-DTC, suggesting a faster adsorption rate.

Adsorption Thermodynamics. Adsorption thermodynamics describe changes in the Gibbs energy (ΔG°), enthalpy (ΔH°), and entropy (ΔS°) during the adsorption process. These parameters are helpful to understand adsorption feasibility and mechanism. The following classical relations are employed to study the adsorption thermodynamics:[46,49,52]

$$\Delta G^\circ = -RT \ln K \quad (7)$$

$$\ln K_c = \frac{\Delta S^\circ}{2.303R} - \frac{\Delta H^\circ}{2.303RT} \quad (8)$$

where R is the gas constant (R = 8.314 J mol/K) and T is the temperature (K). The estimated thermodynamic parameters are placed in Table 4. ΔG° was calculated as −9.689 and −15.504 kJ/mol for MNPs-DTC and MNPs-polyAEMA·DTC, respectively. The negative ΔG° values confirm that adsorption of Hg^{II} by MNPs was a spontaneous process for both systems. The positive values of ΔH° endorse the endothermic nature of the adsorption processes, since an increase in the uptake capacity of particles was observed with an increase in temperature, whereas the positive value of ΔS° illustrates the increasing randomness at the adsorbent surface during the adsorption, which ultimately leads to an increase in the adsorption efficiency. The higher positive value of ΔS° for MNPs-polyAEMA·DTC, compared to MNPs-DTC, predicts a greater affinity between Hg^{II} ions and MNPs-polyAEMA·DTC.

Table 4. Thermodynamic Parameters Associated with the Adsorption of Hg^{II} Ions with MNPs-DTC and MNPs-polyAEMA·DTC[a]

	ΔG° (kJ mol^{-1})	ΔH° (kJ mol^{-1})	ΔS° (kJ mol^{-1} K^{-1})
MNPs-DTC	−9.689	133.315	0.480
MNPs-polyAEMA·DTC	−15.504	191.01	0.693

[a]For a temperature of 303 K.

CONCLUSIONS

We have compared the Hg^{II} removal characteristics of monolayer- and polymer-brush-based dithiocarbamate (DTC)-functionalized magnetic nanoparticles (MNPs) (MNPs-DTC and MNPs-polyAEMA·DTC, respectively). The higher functional group density in the case of MNPs-polyAEMA·DTC was investigated by TEM, TGA, PPPS, and XPS analysis. The adsorption parameters were optimized by studying the effect of the "amount of adsorbent", "contact time", and "temperature" on their Hg^{II} removal capacity. The results confirmed the superiority of MNPs-polyAEMA·DTC over MNPs-DTC, because of its ability to remove almost all the Hg^{II} ions from a 10 ppm solution of Hg^{II} ions.

The linear regression coefficient (R^2) values from Langmuir and Freundlich isotherm model studies suggest that the adsorption behavior of MNPs-DTC is better approximated by the Langmuir isotherm (R^2 = 0.9789), whereas in the case of MNPs-polyAEMA·DTC, it follows the Freundlich isotherm (R^2 = 0.9685). The kinetic behavior of both types of adsorbents followed pseudo-second-order mechanism. The calculation of thermodynamic parameters such as ΔG°, ΔH°, and ΔS° also supported the favorable adsorption behavior of MNPs-polyAEMA·DTC, compared to their monolayer counterpart.

Within the scope of the current study, we demonstrated the synthesis of novel polymer-brush-functionalized MNPs and examined their superior adsorption characteristics. These results may introduce a new direction of applying the highly resourceful field of polymer brushes to produce molecularly designed adsorbents with tunable environmental remediation efficiency and capacity.

ASSOCIATED CONTENT

Supporting Information

Calibration curve of the Hg^{II}-dithizone complex, curves of Langmuir and Freundlich isotherms, curves of kinetic studies, and a video showing magnetic separation are included as Supporting Information. This material is available free of charge via the Internet at http://pubs.acs.org.

AUTHOR INFORMATION

Corresponding Author

*E-mail: basit.yameen@lums.edu.pk.

Notes

The authors declare no competing financial interest.

ACKNOWLEDGMENTS

B.Y. acknowledges financial support from HEC and a start-up grant from LUMS. H.D. and B.Y. thank UNAM, Bilkent University for technical support for XPS, PPMS, TEM, and TGA analysis.

REFERENCES

(1) Darbha, G. K.; Singh, A. K.; Rai, U. S.; Yu, E.; Yu, H.; Chandra Ray, P. *J. Am. Chem. Soc.* **2008**, *130*, 8038−8043.
(2) Zahir, F.; Rizwi, S. J.; Haq, S. K.; Khan, R. H. *Environ. Toxicol. Pharmacol.* **2005**, *20*, 351−360.
(3) Grandjean, P.; Bellinger, D.; Bergman, Å.; Cordier, S.; Davey-Smith, G.; Eskenazi, B.; Gee, D.; Gray, K.; Hanson, M.; Van Den Hazel, P.; Heindel, J. J.; Heinzow, B.; Hertz-Picciotto, I.; Hu, H.; Huang, T. T. K.; Jensen, T. K.; Landrigan, P. J.; McMillen, I. C.; Murata, K.; Ritz, B.; Schoeters, G.; Skakkebæk, N. E.; Skerfving, S.; Weihe, P. *Basic Basic Clin. Pharmacol. Toxicol.* **2008**, *102*, 73−75.
(4) International Programme on Chemical Safety. *Concise International Chemical Assessment Document 50: Elemental mercury and inorganic mercury compounds: Human health aspects*. http://www.who.int/ipcs/publications/cicad/cicads.
(5) European Environment Agency. *Technical Report on "Hazardous substances in Europe's fresh and marine waters"*; 2011; pp 14−16.
(6) United Nations Environment Programme. *Global Mercury Assessment 2013: Sources, emissions, releases, and environmental transport*; 2013; pp 30-44.
(7) Wagner-Döbler, I.; von Canstein, H.; Li, Y.; Timmis, K. N.; Deckwer, W.-D. *Environ. Sci. Technol.* **2000**, *34*, 4628−4634.
(8) Goel, J.; Kadirvelu, K.; Rajagopal, C. *Environ. Technol.* **2004**, *25*, 141−153.
(9) Ali, I. *Chem. Rev.* **2012**, *112*, 5073−5091.
(10) Lu, A.-H.; Salabas, E. L.; Schüth, F. *Angew. Chem., Int. Ed.* **2007**, *46*, 1222−1244.
(11) Cundy, A. B.; Hopkinson, L.; Whitby, R. L. D. *Sci. Total Environ.* **2008**, *400*, 42−51.

(12) Urban, I.; Ratcliffe, N. M.; Duffield, J. R.; Elder, G. R.; Patton, D. *Chem. Commun.* **2010**, *46*, 4583−4585.
(13) Lohse, S. E.; Murphy, C. J. *J. Am. Chem. Soc.* **2012**, *134*, 15607−15620.
(14) Liu, Y.; Su, G.; Zhang, B.; Jiang, G.; Yan, B. *Analyst* **2011**, *136*, 872−877.
(15) Pan, Y.; Du, X.; Zhao, F.; Xu, B. *Chem. Soc. Rev.* **2012**, *41*, 2912−2942.
(16) Love, J. C.; Estroff, L. A.; Kriebel, J. K.; Nuzzo, R. G.; Whitesides, G. M. *Chem. Rev.* **2005**, *105*, 1103−1170.
(17) Jal, P. K.; Patel, S.; Mishra, B. K. *Talanta* **2004**, *62*, 1005−1028.
(18) Hutchison, A. R.; Atwood, D. A. *J. Chem. Crystallogr.* **2003**, *33*, 631−645.
(19) Figueira, P.; Lopes, C. B.; Daniel-da-Silva, A. L.; Pereira, E.; Duarte, A. C.; Trindade, T. *Water Res.* **2011**, *45*, 5773−5784.
(20) Parham, H.; Zargar, B.; Shiralipour, R. *J. Hazard. Mater.* **2012**, *205*−*206*, 94−100.
(21) Antochshuk, V.; Olkhovyk, O.; Jaroniec, M.; Park, I.-S.; Ryoo, R. *Langmuir* **2003**, *19*, 3031−3034.
(22) Starvin, A. M.; Rao, T. P. *J. Hazard. Mater.* **2004**, *113*, 75−79.
(23) Nam, K. H.; Gomez-Salazar, S.; Tavlarides, L. L. *Ind. Eng. Chem. Res.* **2003**, *42*, 1955−1964.
(24) Wang, J.; Zheng, S.; Shao, Y.; Liu, J.; Xu, Z.; Zhu, D. *J. Colloid Interface Sci.* **2010**, *349*, 293−299.
(25) Shariati, S.; Faraji, M.; Yamini, Y.; Rajabi, A. A. *Desalination* **2011**, *270*, 160−165.
(26) Teja, A. S.; Koh, P.-Y. *Prog. Cryst. Growth Charact. Mater.* **2009**, *55*, 22−45.
(27) Shin, S.; Jang, J. *Chem. Commun.* **2007**, *0*, 4230−4232.
(28) Yantasee, W.; Warner, C. L.; Sangvanich, T.; Addleman, R. S.; Carter, T. G.; Wiacek, R. J.; Fryxell, G. E.; Timchalk, C.; Warner, M. G. *Environ. Sci. Technol.* **2007**, *41*, 5114−5119.
(29) Liu, J.-f.; Zhao, Z.-s.; Jiang, G.-b. *Environ. Sci. Technol.* **2008**, *42*, 6949−6954.
(30) Tran, H. V.; Tran, L. D.; Nguyen, T. N. *Mater. Sci. Eng., C* **2010**, *30*, 304−310.
(31) Koehler, F. M.; Rossier, M.; Waelle, M.; Athanassiou, E. K.; Limbach, L. K.; Grass, R. N.; Gunther, D.; Stark, W. J. *Chem. Commun.* **2009**, *0*, 4862−4864.
(32) Zhao, Y.-G.; Shen, H.-Y.; Pan, S.-D.; Hu, M.-Q.; Xia, Q.-H. *J. Mater. Sci.* **2010**, *45*, 5291−5301.
(33) Tural, B. *Clean: Soil, Air, Water* **2010**, *38*, 321−327.
(34) Girginova, P. I.; Daniel-da-Silva, A. L.; Lopes, C. B.; Figueira, P.; Otero, M.; Amaral, V. S.; Pereira, E.; Trindade, T. *J. Colloid Interface Sci.* **2010**, *345*, 234−240.
(35) Halperin, A.; Tirrell, M.; Lodge, T. P. Tethered chains in polymer microstructures. In *Macromolecules: Synthesis, Order and Advanced Properties*, Springer: Berlin and Heidelberg, Germany: 1992; Vol. *100/1*, pp 31−71.
(36) Milner, S. T. *Science* **1991**, *251*, 905−914.
(37) Barbey, R.; Lavanant, L.; Paripovic, D.; Schüwer, N.; Sugnaux, C.; Tugulu, S.; Klok, H.-A. *Chem. Rev.* **2009**, *109*, 5437−5527.
(38) Koenig, A.; Ziener, U.; Schaz, A.; Landfester, K. *Macromol. Chem. Phys.* **2007**, *208*, 155−163.
(39) Elly, C. T. *J.—Water Pollut. Control Fed.* **1973**, *45*, 940−945.
(40) Arias, J. L.; Reddy, L. H.; Couvreur, P. *Langmuir* **2008**, *24*, 7512−7519.
(41) Yuan, W.; Yuan, J.; Zhou, L.; Wu, S.; Hong, X. *Polymer* **2010**, *51*, 2540−2547.
(42) Huang, Y.-F.; Wang, Y.-F.; Yan, X.-P. *Environ. Sci. Technol.* **2010**, *44*, 7908−7913.
(43) Xuan, S.; Hao, L.; Jiang, W.; Gong, X.; Hu, Y.; Chen, Z. *J. Magn. Magn. Mater.* **2007**, *308*, 210−213.
(44) Salman, M.; Athar, M.; Shafique, U.; Din, M. I.; Rehman, R.; Akram, A.; Zulfiqar, A. *Turkish J. Eng. Env. Sci.* **2011**, 209−216.
(45) Sreelatha, G.; Kushwaha, S.; Rao, V. J.; Padmaja, P. *Ind. Eng. Chem. Res.* **2010**, *49*, 8106−8113.
(46) Sarı, A.; Şahinoğlu, G.; Tüzen, M. *Ind. Eng. Chem. Res.* **2012**, *51*, 6877−6886.
(47) Parida, K. M.; Sahu, S.; Reddy, K. H.; Sahoo, P. C. *Ind. Eng. Chem. Res.* **2010**, *50*, 843−848.
(48) Saha, B.; Das, S.; Saikia, J.; Das, G. *J. Phys. Chem. C* **2011**, *115*, 8024−8033.
(49) Wang, S.; Ng, C. W.; Wang, W.; Li, Q.; Li, L. *J. Chem. Eng. Data* **2012**, *57*, 1563−1569.
(50) Liu, T.; Yang, M.; Wang, T.; Yuan, Q. *Ind. Eng. Chem. Res.* **2012**, *51*, 454−463.
(51) Li, X.; Zhou, X.; Mu, J.; Lu, L.; Han, D.; Lu, C.; Wang, M. *J. Chem. Eng. Data* **2011**, *56*, 4274−4277.
(52) Oladoja, N.; Ololade, I.; Idiaghe, J.; Egbon, E. *Cent. Eur. J. Chem.* **2009**, *7*, 760−768.